Separation and Purification Technology 354 (2025) 129134

Contents lists available at ScienceDirect

Separation and Purification Technology

journal homepage: www.elsevier.com/locate/seppur

Electro reduction-recovery of $Au(S_2O_3)_2^{3-}$ within a low concentration range *via* multi-porous activated carbon electrodes

Xuan Zhang [a,b], Weiquan Zhan [c,*], Qizheng Weng [a], Sheng Wang [b], Shaoxian Song [d], José Luis Arauz-Lara [c], Feifei Jia [a,b,**]

[a] Key Laboratory of Green Utilization of Critical Non-metallic Mineral Resources of Ministry of Education, Wuhan University of Technology, Wuhan 430070, Hubei, China
[b] School of Resources and Environmental Engineering, Wuhan University of Technology, Wuhan 430070, Hubei, China
[c] Instituto de Fisica, Universidad Autónoma de San Luis Potosí, Av. Manuel Nava 6, Zona Universitaria, San Luis Potosí 78290, Mexico
[d] Instituto de Metalurgia, Universidad Autónoma de San Luis Potosí, Av. Sierra Leona 550, San Luis Potosí 78210, Mexico

ARTICLE INFO

Editor: G. Chen

Keywords:
Electro reduction-recovery
Low concentration
$Au(S_2O_3)_2^{3-}$
Multi-porous AC electrodes

ABSTRACT

Low-concentration gold recovery from thiosulfate solutions ($Au(S_2O_3)_2^{3-}$) was vital for the application of thiosulfate leaching instead of traditional cyanide leaching in gold industries. Herein, electro reduction-recovery of gold in thiosulfate solutions *via* multi-porous activated carbon (AC) was proposed. Recovery of $Au(S_2O_3)_2^{3-}$ within a low concentration range by multi-porous AC electrodes reached to almost 100 %. Even in the presence of high concentration interferential ions (molar ratio of $S_2O_3^{2-}$ to Au was 300:1), there was not any effect on the recovery. Interestingly, $Au(S_2O_3)_2^{3-}$ was recovered on the surface of multi-porous AC electrodes as the form of gold metal, realizing the recovery and reduction at the same time, which would be prone to shorten the traditional recovery procedure. Besides, the correlation of $Au(S_2O_3)_2^{3-}$ adsorption behaviors and multi-porous AC structure was well studied. Appropriate activation temperature was beneficial for the generation of multi pores together with oxygen functional groups, providing rich activate sites for $Au(S_2O_3)_2^{3-}$ adsorption and reduction. High electric double layer capacity (EDLC) and low charge transfer resistance jointly affected the $Au(S_2O_3)_2^{3-}$ recovery ability. The work provided an approach for gold recovery within a low concentration range in thiosulfate leaching solutions using multi-porous AC electrodes, thus to promote the green development of gold resources.

1. Introduction

As a kind of typical precious metal, gold with excellent stability, electrical conductivity, and catalytic abilitiesis is widely used in jewelry, currency, and high-tech industries [1]. With rapid development of electronic industry, the amount of easily extracted gold ores is dwindling, thus most researches focus on gold ores with low grade [2,3]. Cyanide leaching is the classical gold leaching method in industries for decades [4,5], while it is hard to leach gold ores containing graphite or organic carbon because of "robbed" or absorption by the inherent preobbing minerals [6]. Besides, existence of excessive competition between gold and harmful minerals induces chemical consumption [7,8]. Except the above drawbacks, cyanide leaching faces challenge of its well-known toxicity especially in the era of green development [9,10]. Therefore, it is imperative to propose clean and efficient alternative cyanide leaching method for the development of gold industry.

At present, various non-cyanide leaching methods including thiosulfate, thiocyanate thiourea, and halogen leaching are proposed [11]. Thiourea leaching labelled with a potential carcinogen requires acidic environment and high corrosion resistance of the equipment. Halide owns the disadvantages of strong causticity and needing a great deal of medicine. There exists the limited availability to the temperature and solution pH in thiocyanate leaching process. Among these techniques, thiosulfate leaching is considered as the most promising non-cyanide method and has been demonstrated in the extraction of complex gold ores [12]. Nevertheless, recovering gold from thiosulfate leaching solutions ($Au(S_2O_3)_2^{3-}$) remains significant challenges [13].

Plenty of conventional methods have been applied on gold recovery

* Corresponding author at: Instituto de Fisica, Universidad Autónoma de San Luis Potosí, Av. Manuel Nava 6, Zona Universitaria, San Luis Potosí 78290, Mexico
** Corresponding author at: Key Laboratory of Green Utilization of Critical Non-metallic Mineral Resources of Ministry of Education, Wuhan University of Technology, Wuhan 430070, Hubei, China.
E-mail addresses: zhan_weiquan@163.com (W. Zhan), feifeijia@whut.edu.cn (F. Jia).

https://doi.org/10.1016/j.seppur.2024.129134
Received 1 June 2024; Received in revised form 3 August 2024; Accepted 7 August 2024
Available online 9 August 2024

from thiosulfate leaching solution, such as ion exchange, solvent extraction, precipitation, and adsorption [14], while most of them faced the challenges in low recovery, or high cost, or hard operation. Recently, we proposed catalytic reduction method to achieve in-situ and efficient $Au(S_2O_3)_2^{3-}$ recovery from aqueous solutions based on molybdenum disulfide [15,16], but it is not satisfactory to recover $Au(S_2O_3)_2^{3-}$ under low concentration conditions. Owing to the ongoing exploitation of the rich gold deposits, the remaining low-grade gold ores like sulfide gold ores containing high arsenic, sulfur elements and carbonaceous refractory gold ores are leached with a low concentration of gold, typically less than 10 mg/L [4,17]. In addition, the gold in some electronic wastes and wastewater is with little amount, for example, waste printed circuit boards containing ~0.03 % Au [18], the gold concentration in e-waste recycling wastewater and gold mining wastewater ranged from ppb level to tens of ppm [19,20]. Therefore, developing an efficient method to achieve low-concentration $Au(S_2O_3)_2^{3-}$ recovery is necessary for applying thiosulfate leaching in industries.

Electrodeposition has been applied on $Au(CN)_2^-$ recovery in industries [21] cause the targeted ions can be reduced into particles on electrode, thus to achieve highly gold recovery. Nevertheless, this method hardly recovers $Au(S_2O_3)_2^{3-}$ owing to poor affinity between electrodes and target ions. The properties of electrode materials largely determine the electro sorption capability and reaction rate. If coating materials on the surface of usual electrodes for $Au(S_2O_3)_2^{3-}$ recovery (electro reduction-recovery), $Au(S_2O_3)_2^{3-}$ will be attracted, absorbed, and reduced on electrodes at the same time [22,23]. What's more, the immigration of $Au(S_2O_3)_2^{3-}$ is driven by an external electric field in aqueous solutions, which promotes the adsorption process. Finding an appropriate material served as coating is important for low-concentration $Au(S_2O_3)_2^{3-}$ recovery.

Porous materials have been used in electrosorption of metal ions, like uranium(IV) [24], arsenic(III) [25], lead(II) [26], lanthanum(III) [27] and mercury(II) [28] due to their large specific surface area and rich porous structure. Porous structure of carbon materials can serve as channels for gold ions to penetrate the surface of the activated carbon, facilitate charge transfer and be beneficial for ions storage [29]. Specially, micropore plays a vital role in adsorption and amplification current with its surficial groups [30]. Based on hard soft acids bases theory [31], abundant oxygen-contained groups on the surface of porous materials like C—O, C═O as soft acid will bind with gold complex as soft base.

Titanium plate has been widely used as electrode substrate because of its stable properties, strong acid and alkali resistance, simple processing, easy deformation, repeated use [32]. Among the porous materials, activated carbon (AC) with low price, abundant sources, and stability attracts board attentions [33,34]. Activation is a common way to tune micropore structure of AC [35]. Here, we proposed KOH activation method to enrich micropore structure of AC for efficient electro reduction-recovery of low-concentration $Au(S_2O_3)_2^{3-}$ due to its ability to produce high surface area AC, low environmental pollution, less corrosiveness, lower cost and higher efficiency in the adsorption of heavy metals compared to other activators [36]. This work is helpful to understand the role of micropore in electro reduction-recovery process, and provide a way for improving low-concentration $Au(S_2O_3)_2^{3-}$ recovery.

2. Materials and methods

2.1. Materials

Potassium hydroxide (KOH), sodium hydroxide (NaOH), hydrochloric acid (HCl), ethanol (C_2H_5OH), polyvinylidene fluoride (PVDF), N, N-Dimethylacetamide (DMA, $CH_3CON(CH_3)_2$) were all obtained from Sinopharm Chemical Reagent Co., Ltd, China. Conductive carbon black was bought from the Cabot Co., China. Ammonium thiosulfate ($(NH_4)_2S_2O_3$) was purchased from Aladdin Co., China. Standard gold solution ($HAuCl_4$, 1000 mg/L) was obtained from Well Group Scientific Ltd, USA. The walnuts as the biomass precursors for AC were bought from Zhiyin Store, Wuhan Province, China. The deionized water used in this work was produced by Millipore Milli-Q Direct 8/16 water purification system.

2.2. Synthesis of multi-porous AC

Multi-porous AC was prepared according to previous literatures [37,38]. AC was obtained through carbonizing walnut shell powder at 5 °C/min to 400 °C under nitrogen atmosphere for 1 h. After being washed by ethanol and deionized water, the powder was dried by freeze-drying at −20 °C in vacuum for 24 h, named as AC0. Based on the original AC materials, multi-porous AC was synthesized by activation method. AC0 and KOH in a mass ratio of 1:3 was mixed and grinded, and then the mixture was heated at 5 °C/min to a certain temperature under nitrogen atmosphere for 2 h. After cooling to room temperature, the obtained products were washed with HCl and deionized water. Finally, through freeze-drying, multi-porous AC samples were prepared. According to the synthesis temperature, 500 °C, 600 °C, 700 °C, and 800 °C, samples synthesized were named as multi-AC1, multi-AC2, multi-AC3, and multi-AC4, respectively.

2.3. Fabrication of multi-porous AC electrodes

Multi-porous AC, conductive carbon black, and polyvinylidene fluoride (dissolved in the DMA, 12.5 g/L) in a mass ratio of 8:1:1 were mixed, and then the mixture was coated on the surface of titanium plate. Afterwards, the obtained electrodes were heated at 60 °C for 6 h to remove the residual organic solvent. Lastly, the electrodes were immerged into the deionized water for 12 h to remove impurities and heated at 60 °C for 3 h to shape.

2.4. Electro Reduction-recovery of $Au(S_2O_3)_2^3$

$Au(S_2O_3)_2^{3-}$ solution was prepared like previous literatures [22,39]: $(NH_4)_2S_2O_3$ and $HAuCl_4$ were added into deionized water while the pH was maintained at 10. The prepared solution was poured into a 200 mL reaction cell (Fig. S1). An external current was connected to the both multi-porous AC electrodes, while the reaction cell was circulated at 45 rpm by a peristaltic pump.

During the recovery process, solution samples were collected at different time intervals, being filtered through a 0.22 μm filter membrane to remove insoluble impurities. The concentration of Au was detected by an atomic absorption spectroscopy. Recovery (R, %) and adsorption capacity (Q, mg/g) were calculated through the following formulas to evaluate the recovery performances:

$$R = \frac{C_0\text{-}C_t}{C_0} \times 100\% \quad (1)$$

$$Q = \frac{C_0V\text{-}C_tV_t}{m} \quad (2)$$

Where C_0 was Au concentration at the initial time, mg/L; C_t was residual Au concentration at t moment, mg/L; V was the initial volume of solution, L; V_t was the residual volume at t moment, L; m was mass of coated samples on titanium plate, mg.

Conditional experiments including molar ratio of $S_2O_3^{2-}$ to Au, initial concentration, voltage, electrodes-distance and pH were considered to investigating the recovery performance. HNO_3 and NaOH was used to adjust the pH of solutions. Molar ratio of $S_2O_3^{2-}$ to Au from 3:1 to 300:1 was studied at concentration of 5 mg/L, voltage of 1.2 V, pH of 10, electrodes-distance of 5 mm. Initial concentration from 1 to 10 mg/L was researched at molar ratio of $S_2O_3^{2-}$ to Au of 3:1, voltage of 1.2 V, pH of 10, electrodes-distance of 5 mm. Applied voltage in the range of 0–1.6 V was studied at molar ratio of $S_2O_3^{2-}$ to Au of 3:1, concentration of 5

mg/L, pH of 10, electrodes-distance of 5 mm. Effect of distance between electrodes including 2, 5, 8, 11, and 14 mm was investigated at concentration of 5 mg/L, voltage of 1.2 V, pH of 10. The pH was researched at concentration of 5 mg/L, voltage of 1.2 V, electrodes-distance of 5 mm.

2.5. Analyses

X-ray diffraction (XRD) with Cu-Kα radiation was applied on detecting the crystal structure, D8 Advance, Bruker AXS, Germany. Raman was provided for studying the atomic bond structure of samples, INVIA Renishaw, England. Thermogravimetric analysis (TG) and differential scanning calorimetry (DSC) was used to obtain the thermal stability, composition, and physical properties of samples through the Simultaneous thermal analyzer, STA449F3 Jupiter, Germany. The scanning electron microscopy (SEM) and energy-dispersive X-ray spectroscopy (EDS) images were obtained using Phenom ProX G6, Netherlands. Transmission electron microscopy (TEM) was used to observe the morphology and microstructure, JEM-F200 microscope, Japan. The chemical element state was determined by X-ray photoelectron spectroscopy (XPS), Thermo Scientific K-alpha, America. Distribution of pore structure and adsorption and desorption isotherms was studied by the Brunauer-Emmett-Teller (BET), V-Sorb X800, China. Atomic absorption spectrophotometer was employed to measure the element concentration, Agilent 280FS AA, USA. The Zeta potentials of samples were detected by Zetasizer Zeta-nano, ZEN3690, China.

2.6. Electrochemical measurements

Electrochemical characteristics of electrodes including cyclic voltammetry (CV) and electrochemical impedance spectroscopy (EIS) in a 1 M Na_2SO_4 or 5 mg/L $Au(S_2O_3)_2^{3-}$ were performed in three electrodes system through the electrochemical station, VersaSTAT-450, PAR, America. The Pt flake, mercury-mercury oxide electrode and AC/Ti were used as the counter electrode, reference electrode, and working electrode, respectively. CV test was scanned from 1 to 100 mV/s. The frequency range of EIS test was acquired from 0.01 to 10,000 Hz with an open circuit at an AC amplitude of 10 mV. The specific capacitance (C, $F{\cdot}g^{-1}$) of electrodes according to CV curves was calculated by the following equation:

$$C = \frac{\int IdV}{2mv\Delta V} \quad (3)$$

Where I was the current density, A; m was the mass of materials, g; v was the scan rate in CV experiment, $V{\cdot}s^{-1}$; ΔV was the operating voltage difference, V.

3. Results and discussion

3.1. Synthesis of Multi-Porous AC

TG-DSC analysis of AC0 was obtained in Fig. 1 to understand the possible reaction during activation process. It was obvious that there were three significant mass variation stages [40]. The first stage with 2.60 % mass reduction from normal temperature to 120 °C was due to the dehydration drying. Next step arising at temperature between 120 °C and 380 °C with 5.34 % mass loss involved the breakdown of cellulose, lignin, and hemicellulose. Meanwhile, amounts of gases, such as CO, CO_2, and CH_4, were produced and released to create pores in AC. The third stage with 19.40 % mass loss from 380 °C to 700 °C was resulted from the pyrolysis of lignin with a relatively slow rate. The last stage from 700 °C to 1000 °C with just 3.61 % mass loss was a slow decomposition stage, demonstrating that the sample was hardly variable during this stage. Therefore, most multi-porous AC samples were prepared at the temperature of third stage to gain more micropores.

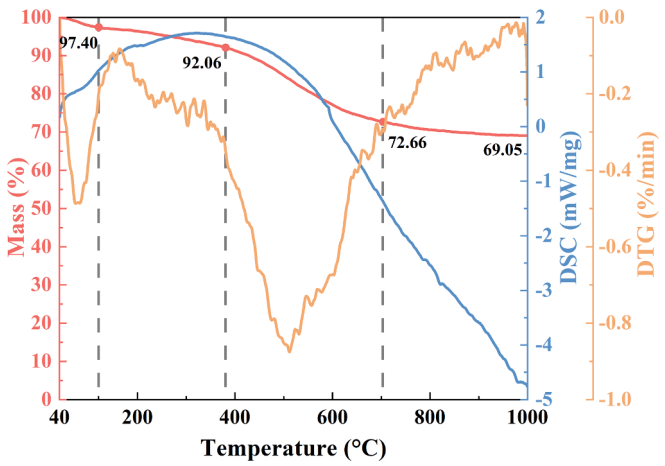

Fig. 1. TG, DSC, and DTG spectra of AC0.

3.2. Microstructure characterization

Crystal structure of samples was detected by XRD (Fig. 2a), and the characteristic diffraction peaks at around 21.8° and 42.4° could be ascribed to the (002) and (100) planes of typical graphitic structure [41]. It was seen that the (002) diffraction peak slightly shifted to lower angle and become broader as increasing the activation temperature, which was attributed to the collapse of microporous structure and graphitization during activation [42]. Among them, multi-AC3 and multi-AC4 exhibited low intensity of the (002) diffraction peak, demonstrating a relatively high porosity [43]. Higher activation temperature, more structural collapse was intensified and less graphitic structure remained. As a result, the samples showed a partial graphitic structure inclined to amorphous carbon. This phenomenon was also verified by Raman results (Fig. 2b). D-band at the peaks of ~1325 cm^{-1} represented the defect of AC, while G-band at ~1590 cm^{-1} meant the degree of carbonization. The intensity ratio of D-band and G-band (I_D/I_G) was an evaluation of defective degrees in carbon structure [44]. It was notable that all samples had a rather low I_D/I_G ratio, endorsing their partially graphitic structures. The intensity ratio of multi-porous AC was higher than that of AC0, being resulted from the structural collapse and erosion by KOH activation. Also, due to the change of surface stress, D-band shifted to lower position while G-band moved to higher position under higher activation temperature. The higher activation temperature, the disorder samples, becoming with a small amount of ordered graphene stacks [43].

3.3. Chemical compositions

Chemical compositions of porous AC was further analyzed by XPS (Fig. 3a-c), The full survey XPS spectrum (Fig. 3a) detected signals of C and O elements, reflecting the composition of the sample. Peaks located at ~284.8, ~286.0, ~288.5, and ~290.6 eV can be ascribed to C—C, C—O, COOR, and Π − Π* groups in C 1*s* spectra (Fig. 3b), respectively [45]. The O 1*s* spectrum in Fig. 3c devaluated into two peaks at ~532.1 and ~533.5 eV was C═O and C—O oxygen-containing functional group respectively, which may improve the wettability and active sites for reaction [46].

3.4. Morphology

Morphologies of multi-porous AC were characterized by SEM and TEM, and they exhibited diverse dimensions of pores. AC0 (Fig. 4a) without activation was relatively smooth, uniform, and consisted of large pores while the microporous was less. The surface of multi-AC1 (Fig. 4b) with activation temperature of 500 °C became rough, and a

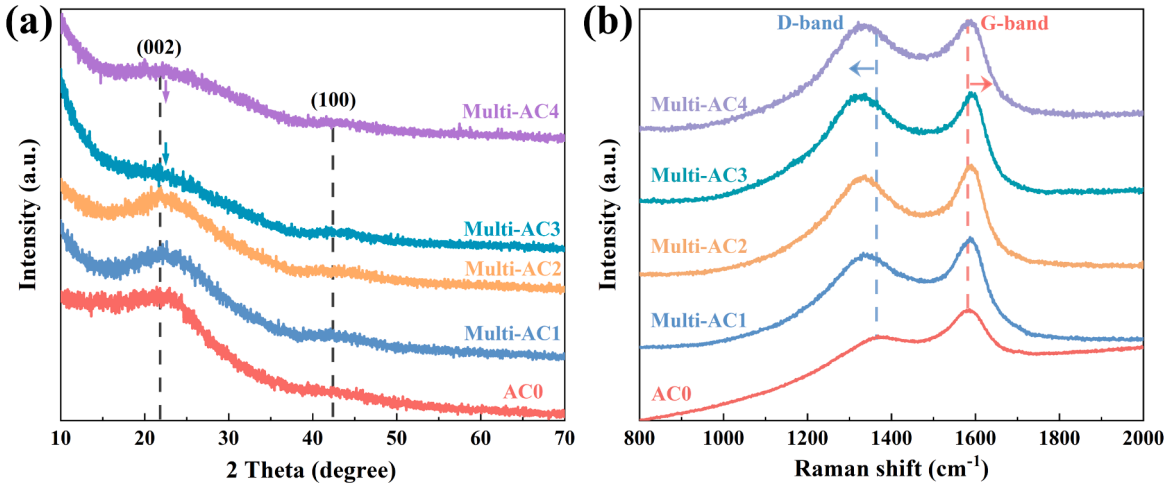

Fig. 2. (a) XRD patterns and (b) Raman spectra of multi-porous AC.

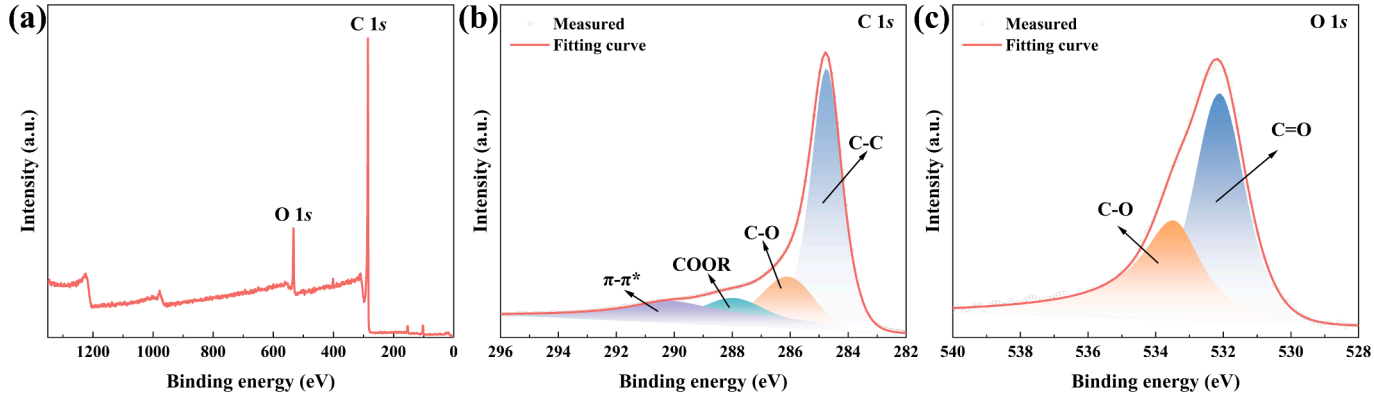

Fig. 3. XPS (a) survey, (b) C 1*s*, and (c) O 1*s* spectrum of multi-porous AC.

lot of relatively small pores were generated. With the rising of the activation temperature, a widespread porous web was created on the surface of multi-AC2, multi-AC3, and multi-AC4 (Fig. 4c-e) originated from the etching of KOH [47,48]. By the close views, it revealed that the surface was abundant with slit-shaped and wedge-shaped pore structure, which would be desirable for absorption [49]. The hierarchical porous structure with large amount of mesopores and micropores co-reside on the wall of a macropores appeared on multi-AC4 (Fig. 4d), revealing that certain activation temperature generated richest structure.

Further, HRTEM was applied to investigate the microstructure of multi-porous AC (Fig. 5a-c), and it showed the disordered region from amorphous carbon. In Fig. 5c, the close view exhibited amounts of micrspores. TEM and corresponding EDS mappings were visible in Fig. 5d-f, which demonstrated that multi-porous AC was consist of entirely C and O element. The micro signal of O element might be ascribed to the existence of oxygen-containing functional groups.

3.5. Porous structure

Distribution of pore structure and adsorption and desorption isotherms was studied by the specific surface area analyzer under a nitrogen atmosphere with a 9 h pretreatment at 100 °C for degassing. Surface area was relevant with the active sites for $Au(S_2O_3)_2^{3-}$ interaction, and the results were given in Fig. 6a. AC0 without activation possessed the lowest surface area of only 2.2 m^2/g. After activation, the surface area was obviously improved, especially multi-AC3 with the highest specific surface area of 2783.3 m^2/g. N_2 adsorption − desorption experiments were performed to research the type of porous structure (Fig. 6b). The step line at a low relative pressure of $p/p_0 < 0.1$ suggested the presence of a large fraction of micropores while the hysteresis loop at a relatively high pressure of around $p/p_0 > 0.8$ indicated the mesoporous structure [50]. All the curves were an intermediate types IV isotherms behavior with H4 hysteresis loops, verifying that the samples had both micropores and mesopores [51]. In Fig. 6c, the cumulative pore volume revealed that AC0 without activation showed the lowest pore volume 69. 7×10^{-3} cm^3/g while the multi-AC3 sample exhibited the highest pore volume of 1560.5×10^{-3} cm^3/g. The above results demonstrated that surface area and porous structure could be tuned by adjusting the activation temperature, which would in turn affecting the electrochemical behaviors.

Different pore size worked in various ways during the absorption process. The presence of macropores and large mesopores facilitated ion diffusion, whilst small mesopores and micropores increased ion-accessible surface area and significantly contributed to adsorption capacity. Pore diameter distribution of various AC was given in Fig. 6d. It could be seen that increasing activation temperature enhanced the mesopores and micropores volume of AC, especially micropores. With the activation temperature increasing, the content of micro-, and mesopores initially increased and then declined but the transition temperature was different. Enhancing activation temperature was beneficial for the formation of porous structure of activated carbon, while the pores content decreased when the activation temperature excessed to a certain value because of the degradation of walls [52,53]. When the size of the micropores was comparable to the ion size, the micropores made maximum contribution to the EDLC due to high electro absorption originated from the strong interaction of ions with the pore in wall [54].

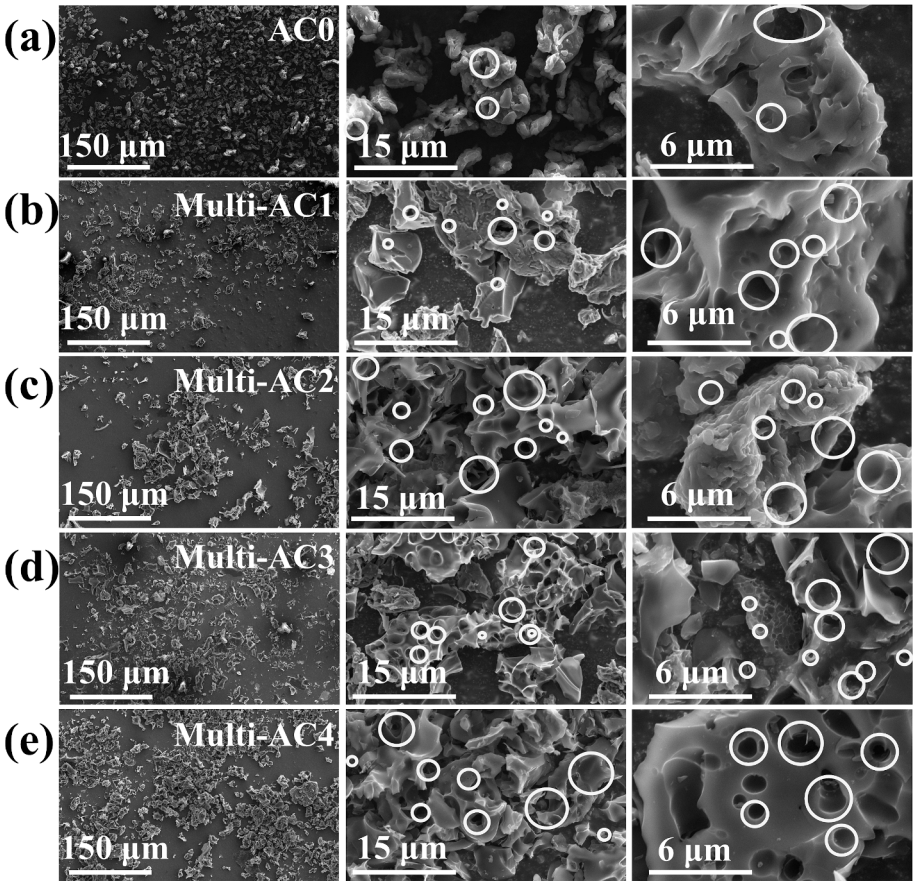

Fig. 4. SEM images of multi-porous AC under different enlarged scale:(a) AC0, (b) multi-AC1, (c) multi-AC2, (d) multi-AC3 and (e) multi-AC4.

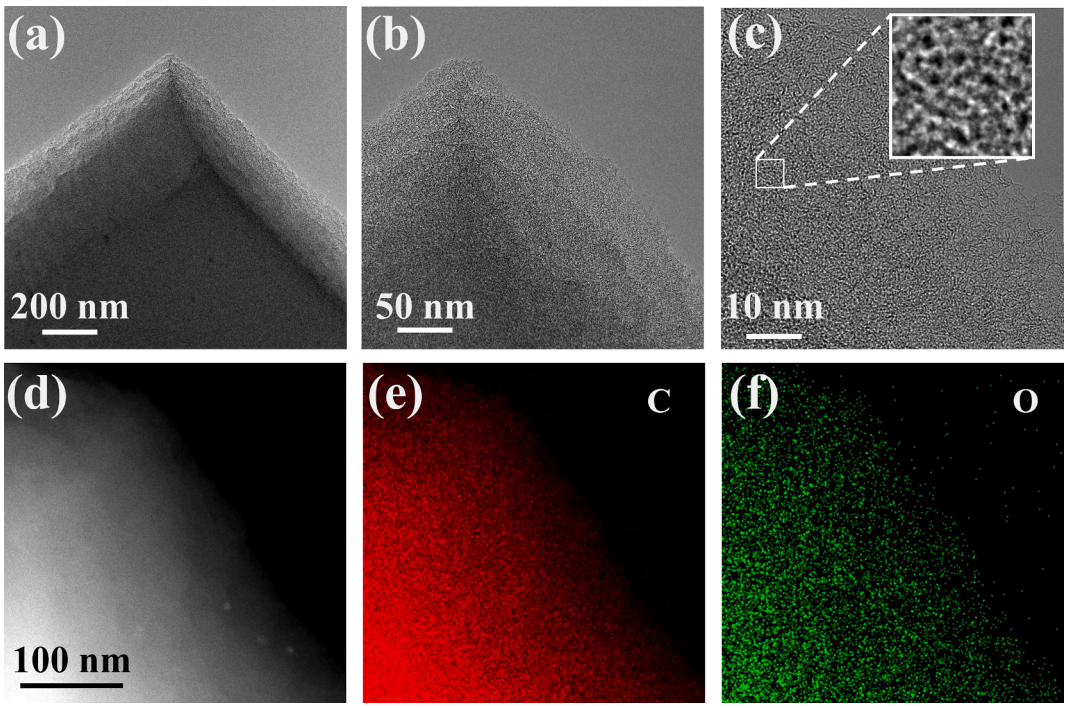

Fig. 5. (a-c) HRTEM images under different magnification of multi-porous AC. (d) TEM image and corresponding EDS mappings: (e) C and (f) O element of multi-porous AC.

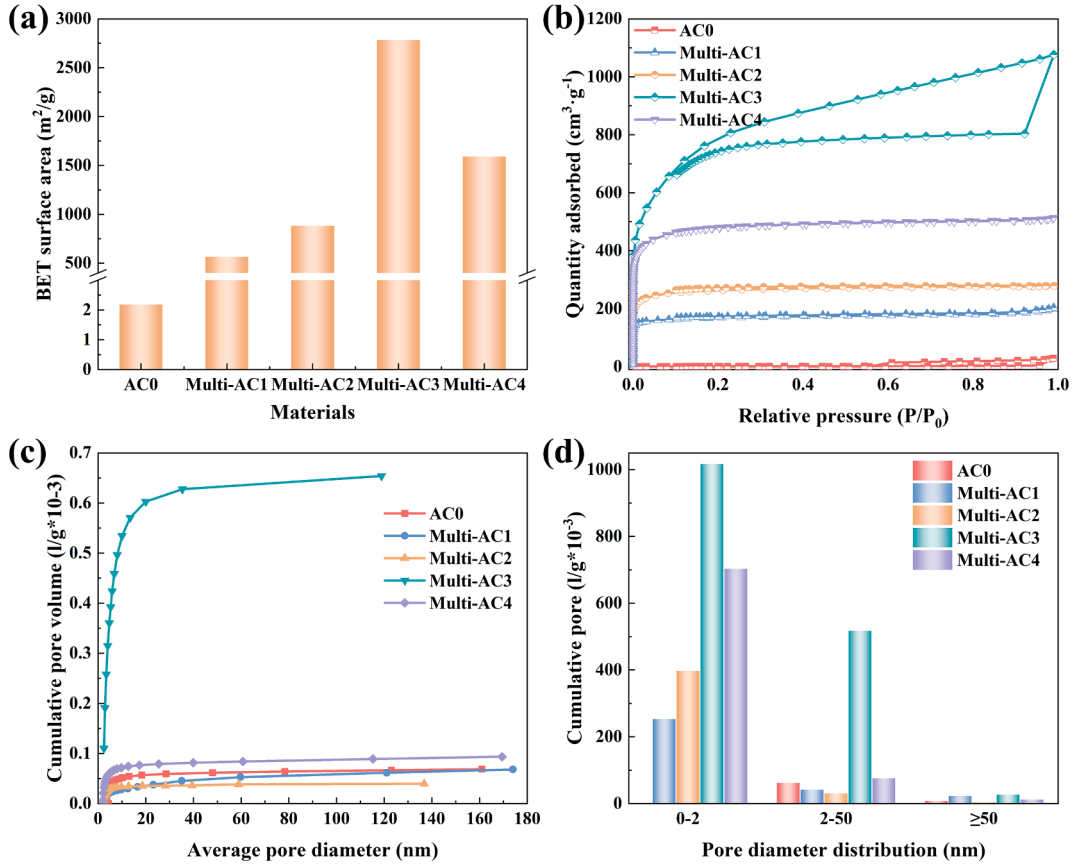

Fig. 6. (a) BET, (b) N_2 isotherm absorption–desorption curves, (c) cumulative pore volume, and (d) pore diameter distribution of multi-porous AC.

Consequently, the improved micropores and mesopores would facilitate the electro reduction-recovery of $Au(S_2O_3)_2^{3-}$.

3.6. *Electro Reduction-Recovery of $Au(S_2O_3)_2^{3-}$*

Low-concentration $Au(S_2O_3)_2^{3-}$ recovery performances through electro reduction-recovery *via* multi-porous AC were studied. During the recovery process, AC was coated on a titanium plate as both the cathode and anode. For comparison, the recovery abilities of Ti-plate electrode and AC electrode as cathode or anode or both were explored (Fig. 7a). The AC as both electrodes performed a largest recovery, more than 1.5-, 2.5-, 5- folds than AC electrode as a cathode or anode, or Ti-plate electrode respectively, demonstrating that the cathode was the main place for gold reduction reaction, while the AC electrodes as anode can promote ion immigration and accelerate the adsorption and reduction process. Electrical double layer can be formed at the both AC electrodes between the electrode material surface and the solution, and facilitate the storage of ions and the interaction between the electrode and ions [55].

The adsorption capacity and recovery (Fig. 7b and c) were obviously improved after activation through comparing multi-porous AC and AC0. Grown the activation temperature, the adsorption capacity and recovery clearly enhanced, while little decrease in multi-AC4 was due to the collapse of the pores. To gain the insight of adsorption process, Webber-Morris dynamics model (Eq. (4) was applied to study the kinetics ion diffusion processes in electro reduction-recovery process, and corresponding fitting data were exhibited in Table 1.

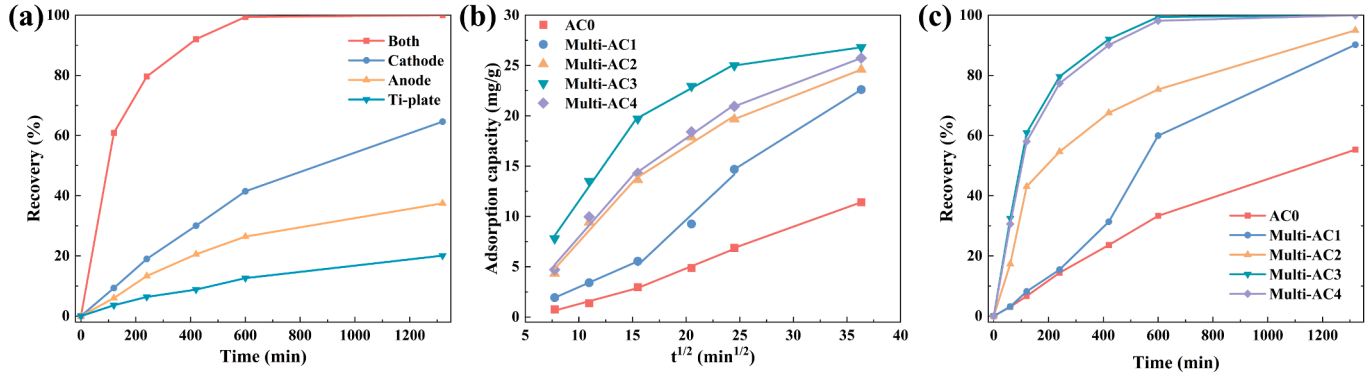

Fig. 7. (a) Recovery performance of Ti-plate electrode and AC electrode as cathode or anode or both, (b) adsorption capacity and (c) $Au(S_2O_3)_2^{3-}$ recovery by various multi-porous AC electrodes.

Table 1
Fitting parameters of $Au(S_2O_3)_2^{3-}$ reduction-recovery steps on AC electrodes descripted by Webber-Morris dynamics model.

Materials	Contact			Internal diffusion		
	k_1	C_1	R_1^2	k_2	C_2	R_2^2
AC0	0.289	−1.592	0.988	0.432	−3.796	0.997
Multi-AC1	0.467	−1.690	1	1.003	−10.395	0.985
Multi-AC2	1.184	−4.373	0.988	0.677	3.414	0.986
Multi-AC3	1.525	−3.712	0.997	0.592	10.623	0.998
Multi-AC4	1.220	−4.246	0.988	0.741	2.943	0.997

$$q_t = k_i t^{1/2} + C \quad (4)$$

Where t was the reaction time, min; q_t was the adsorbed Au at t moment, mg/g; k_i was the rate constants, min^{-1}; C was the constant.

After being fitted, the adsorption process was divided into three steps, surface contact, diffusion, and balance. The fitting curve didn't pass through the origin data, revealing that the adsorption process was controlled by the internal diffusion and other adsorption stages. For the first step, $Au(S_2O_3)_2^{3-}$ diffused rapidly to the surface of electrodes under the synergistic forces of electric field force, concentration gradient driving force, and attraction force from electrode. k_1 of multi-AC4 electrodes was highest, being resulted from strong interaction between multi-AC4 and $Au(S_2O_3)_2^{3-}$. As for k_2 of multi-AC4, it decreased but still reached a high place, that was the reason that macroporous and mesoporous structures provided efficient ion transport paths. AC0 with the most macropores proportion exhibited the largest k_2. The third step was the balance due to saturation of active sites, and smallest slope of multi-AC4 exhibited the best recovery performance. The results showed that the mesopores and macropores paved a way for ion diffusion, and micropores provided abundant active sites for $Au(S_2O_3)_2^{3-}$ adsorption. Accordingly, the recovery using various multi-porous AC electrodes shows similar tendency with that in adsorption capacity results.

Additionally, the recovery performance of $Au(S_2O_3)_2^{3-}$ from a practical thiosulfate leaching solution was investigated (Fig. S2). The gold ore obtained from Shanxi province (China) was leached in copper-ammonia-thiosulfate system with an initial gold concentration of 8.13 mg/L. After 1320 mins, the gold recovery achieved to 99.48 % with adsorption capacity of 55.45 mg/g. Compared with previous experiments carried out with a low gold concentration shown in Table 2, this work achieved efficient recovery of $Au(S_2O_3)_2^{3-}$.

Table 2
Comparison of $Au(S_2O_3)_2^{3-}$ adsorption capacity and recovery with previous literatures.

Adsorbents	Initial concentration (mg/L)	Adsorption capacity (mg/g)	Recovery (%)	Reference
Ag/MoS_2	5	Not reported	96.67	[56]
Cu-TFT-Him	8	Not reported	95	[57]
Walnut shells charcoal	10	42.9	95	[22]
1-methyl-5-mercapto-1,2,3,4-tetrazole-impregnated activated carbon	10	1.9	94	[58]
Polyether sulfone /polym-phenylenediamine membrane	10	91.19	82.53	[59]
Modified magnetic nanoparticles	20	3.580	90	[60]
Cupric ferrocyanide-impregnated activated carbon	100	1.474	75	[61]
Thiol-ene photoclick hydrogels	100	118.8	96.3	[62]
MoS_2/MXene/Ag	100	52	99	[63]
Multi-porous AC	1	6.23	95.41	This work
Multi-porous AC	5	26.81	100	This work
Multi-porous AC	15	75.53	97.57	This work

3.7. Au state after $Au(S_2O_3)_2^{3-}$ recovery

Fig. 8a-d presented SEM images and corresponding EDS mappings of multi-porous AC electrodes after $Au(S_2O_3)_2^{3-}$ recovery. It revealed that the similar morphology with multi-porous AC before reaction. The small particles on the surface of multi-porous AC were covered with Au element in Fig. 8d, indicating the generation of gold particles on the electrodes after recovery.

Furthermore, XPS was carried out to study gold-containing substance after recovery on multi-porous AC in Fig. 9. Appeared Au peaks on XPS survey (Fig. 9a) showed the recovery of gold from thiosulfate solutions. There wasn't obvious change in peaks of C 1*s* (Fig. 9b) and O 1*s* (Fig. 9c) spectrum, which revealed nonexistence of chemical reaction. Au 4*f* spectrum (Fig. 9d) divided into two peaks at 88.2 and 84.5 eV was belonging to Au^0, indicating that the recovery state of $Au(S_2O_3)_2^{3-}$ was gold metal. The possible reactions in cathode (Eq. (5)) and anode (Eq. (6)) happened could be given like this.

$$Au(S_2O_3)_2^{3-} + e^- \rightarrow Au + 2S_2O_3^{2-} \quad (5)$$

$$2S_2O_3^{2-} - 2e^- \rightarrow S_4O_6^{2-} \quad (6)$$

Therefore, above results confirmed the reduction and recovery of Au $(S_2O_3)_2^{3-}$ together on multi-porous AC electrodes, thus the process was called as electro reduction-recovery method.

3.8. Conditional experiments

Conditional experiments of $Au(S_2O_3)_2^{3-}$ recovery including molar ratio of $S_2O_3^{2-}$ to Au, initial concentration, applied voltage, pH, and electrodes-distance were carried out. It is necessary to study the effect of increasing the amount of $S_2O_3^{2-}$ on recovery because $S_2O_3^{2-}$ as a kind of complex ions with similar property of $Au(S_2O_3)_2^{3-}$ will be a main competitive ion for $Au(S_2O_3)_2^{3-}$ recovery and the amounts of $S_2O_3^{2-}$ are often excessive in the real-world thiosulfate leaching gold process [64]. Fig. 10a showed that during the molar ratio of $S_2O_3^{2-}$ to Au changed from 3:1 to 300:1, the recovery performance remained at a high level, demonstrating that even in the presence of high concentration interferential ions, there was not any effect on the recovery. As seen, recovery under low concentration condition achieved ~ 100 % (Fig. 10b), and adsorption capacity was enhanced from 6.23 to 75.53 mg/g with increasing initial concentration, which demonstrated the great potential in applying multi-porous AC electrodes in $Au(S_2O_3)_2^{3-}$ recovery. Applied voltage as a critical parameter directly influenced the efficiency and mechanism of $Au(S_2O_3)_2^{3-}$ recovery (Fig. 10c). Applied voltage created an external electric field to force $Au(S_2O_3)_2^{3-}$ to migrate towards the oppositely charged electrode and then into the pores of the electrodes. Applied voltage greatly improved recovery ability for $Au(S_2O_3)_2^{3-}$ *via* multi-porous AC electrodes compared with that without applied voltage. When applied voltage reached 1.2 V, the recovery and adsorption capacity increased to ~ 100 % and 26.81 mg/g, respectively. However, there was a declined recovery and adsorption capacity at 1.6 V due to the occurrence of an electrolytic water reaction. The effect of electrodes-distance on $Au(S_2O_3)_2^{3-}$ recovery was illustrated in Fig. 10d. When the electrodes-distance was 2 mm, $Au(S_2O_3)_2^{3-}$ recovery was at a low level, which was owing to the slow solution convection. Expanding the distance, $Au(S_2O_3)_2^{3-}$ recovery got a high value, especially at 5 mm, being caused by the enhanced ion migration towards the electrodes. However, small declined $Au(S_2O_3)_2^{3-}$ recovery as continue enhancing electrodes-distance because ohmic losses in two electrodes. Effect of pH on Au

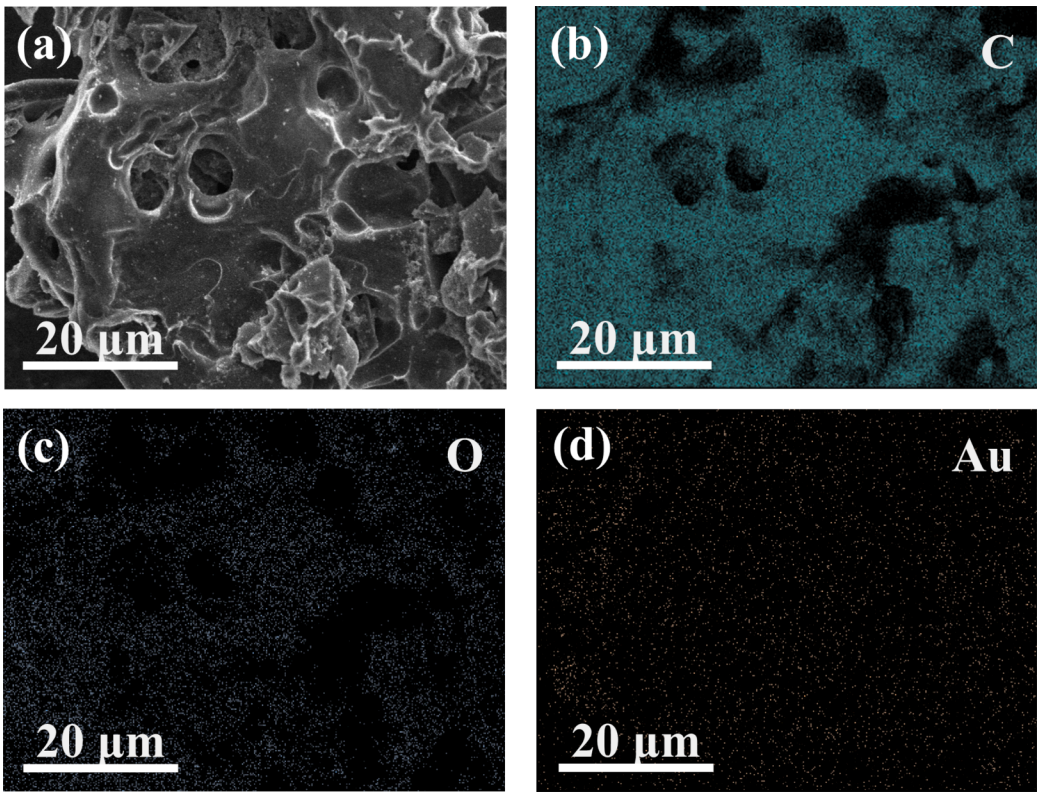

Fig. 8. (a) SEM image and EDS mappings: (b) C, (c) O, and (d) Au element of multi-porous AC electrodes.

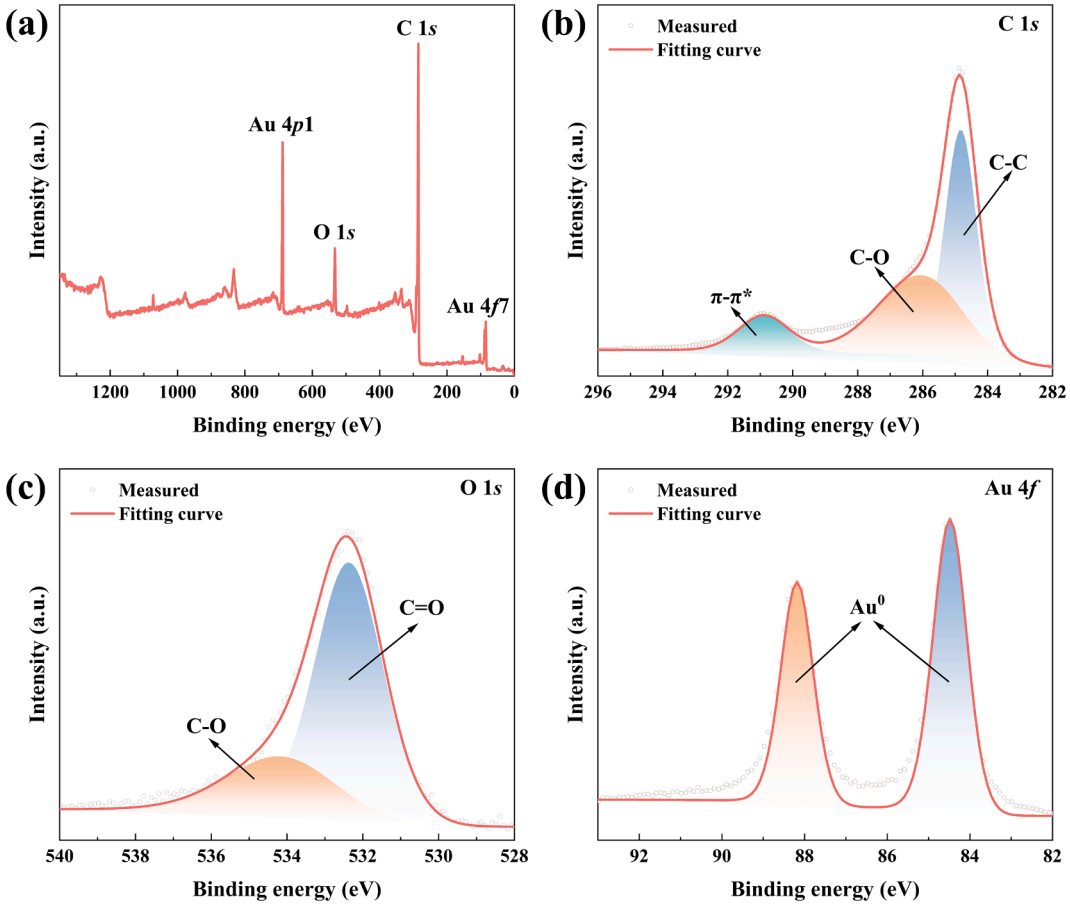

Fig. 9. XPS (a) survey, (b) C 1*s*, (c) O 1*s*, and (d) Au 4*f* spectrum of multi-porous AC electrodes after $Au(S_2O_3)_2^{3-}$ recovery.

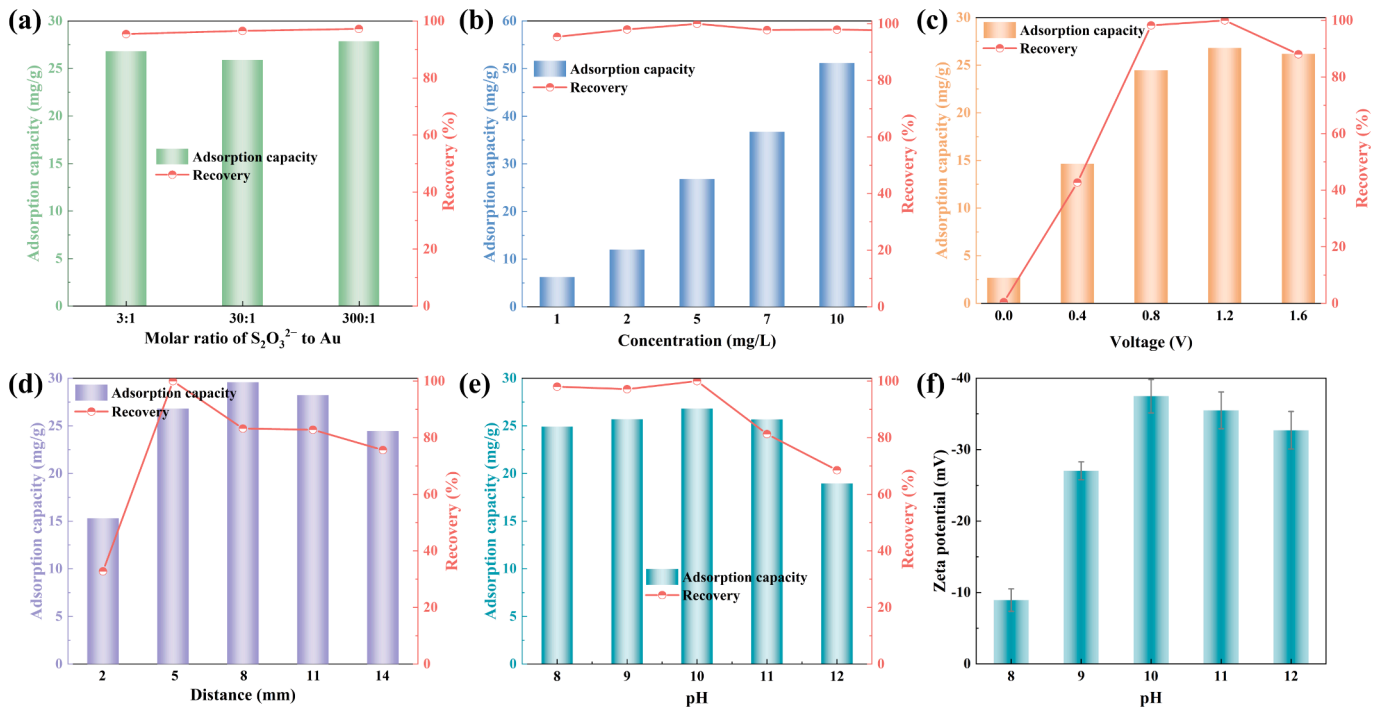

Fig. 10. Effects of conditional parameters on $Au(S_2O_3)_2^{3-}$ recovery by multi-porous AC electrodes: (a) molar ratio of $S_2O_3^{2-}$ and Au, (b) initial concentrarion, (c) applied voltage, (d) electrodes-distance, and (e) pH solution. (f) Zeta potential of multi-porous AC at various pHs condition.

$(S_2O_3)_2^{3-}$ recovery was employed in Fig. 10e. It showed that a high recovery was obtained from 8 to 10, but being dropped at the value of 11 and 12, which may due to the competition of $Au(S_2O_3)_2^{3-}$ and hydroxyl ions on the active sites (Fig. 10f) [65].

3.9. Electro reduction-recovery behaviors

Electrochemical behaviors of electrodes were conducted to reveal adsorption, reduction, and ions transfer process. Fig. 11a illustrated the CV curves of $Au(S_2O_3)_2^{3-}$ solution on AC0 and various multi-porous AC electrodes. All the electrodes exhibited a reduction peak from −0.25 to −0.75 eV, indicating the existed reduction reaction of $Au(S_2O_3)_2^{3-}$ to Au^0. The specific capacitance was calculated based on the area of CV curves (Fig. S3), which showed that largest value on multi-AC3 revealed the violentest reaction (Fig. 11b), thus to be beneficial for $Au(S_2O_3)_2^{3-}$ reduction and recovery.

In order to reveal the EDLC ability of AC0 and multi-porous AC electrodes, CV at different scan rate and EIS curves of electrodes in Na_2SO_4 solution were performed. Electrodes exhibited rectangular shape without obvious redox peaks (Fig. S4), suggesting the existence of EDL and enough time for ions diffuse. According to the specific capacitance (Fig. 12a) calculated from CV curves, the multi-AC3 performed the largest calculated specific capacitance which was controlled by the micropore volume but independent of the mesopores volume [66], showing the highest capacitance for ion storage. Improved ion capacity was relevant with the charged electrodes since the strong electrostatic interaction between Na^+ and negative multi-porous electrodes (Fig. S5). Multi-porous electrodes with more charges improve the EDLC ability. Ion diffusion was tested by EIS (Fig. 12b), the smaller diameter of semicircle meant the lower charge transfer resistance. With more micropores and mesopores, the reactive sites were richer and the transfer resistance was lower, and multi-AC3 possessed relatively smallest impedance and lowest resistance, resulting in a best performance for Au $(S_2O_3)_2^{3-}$ ions transfer and recovery.

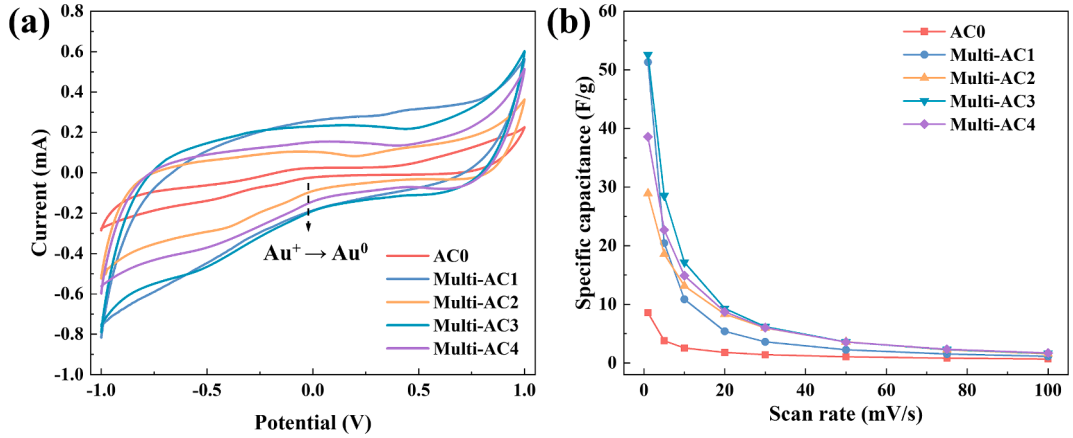

Fig. 11. (a) CV curves and (b) the specific capacitance at different scan rate of AC0 and various multi-porous AC electrodes in $Au(S_2O_3)_2^{3-}$ solution.

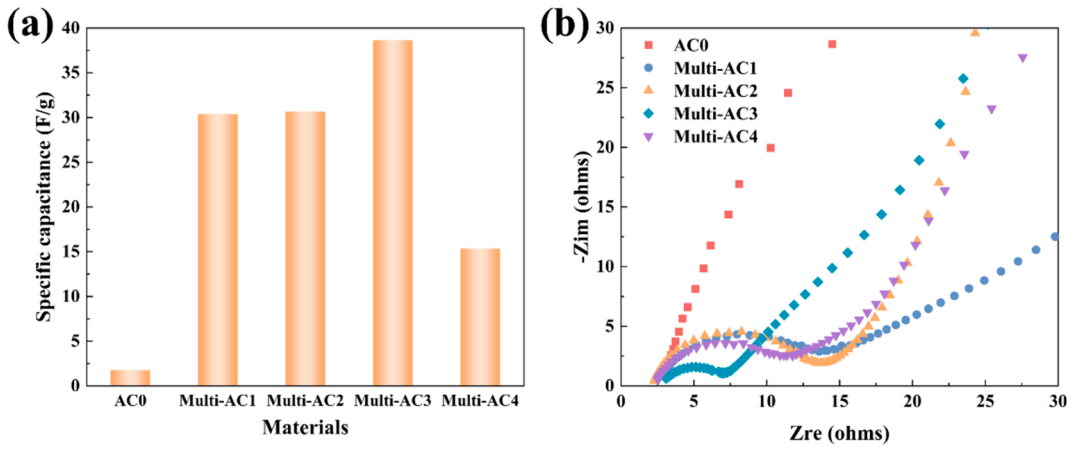

Fig. 12. (a) The specific capacitance and (b) EIS curves of multi-porous AC in Na_2SO_4 solution.

4. Conclusions

In conclusion, low concentration of $Au(S_2O_3)_2^{3-}$ was efficiently reduced and recovered at the same time using multi-porous AC electrodes. Various multi-porous AC were synthesized by adjusting activation temperature based on walnut shell raw materials. $Au(S_2O_3)_2^{3-}$ recovery reached ~ 100 % under a low concentration range and the highest adsorption capacity achieved to 75.53 mg/g. Even under the presence of interferential ions, adsorption capacity and recovery were not affected. Operational parameters were performed to optimize the recovery experiments. High applied voltage and pH were beneficial for the recovery, while low electrodes-distance weakened the recovery because of the slow convection. Appropriate EDLC and ion transfer resistance facilitated the adsorption capacity and reduction process of $Au(S_2O_3)_2^{3-}$. This study offers valuable insights into the design of porous AC electrodes for the electro reduction-recovery of $Au(S_2O_3)_2^{3-}$, and the findings contribute to the sustainable and efficiency gold recovery applications, with implications for the broader field of resource recovery.

CRediT authorship contribution statement

Xuan Zhang: Writing – original draft, Formal analysis, Methodology. **Weiquan Zhan:** Writing – review & editing, Supervision, Methodology. **Qizheng Weng:** Software, Investigation. **Sheng Wang:** Supervision, Methodology. **Shaoxian Song:** Data curation. **José Luis Arauz-Lara:** Conceptualization. **Feifei Jia:** Data curation, Supervision.

Declaration of competing interest

The authors declare that they have no known competing financial interests or personal relationships that could have appeared to influence the work reported in this paper.

Data availability

No data was used for the research described in the article.

Acknowledgements

The work is financially supported by the National Key Research and Development Program of China (2021YFC2900900), and the Natural Science Foundation of Hubei Province (ZRJQ2022000195). Zhan gratefully acknowledges the Consejo Nacional de Humanidades Cienciasy Tecnologías (CONAHCYT) of Mexico for offering him the scholarship under the grant No. 813934 during his Ph.D. studies.

Appendix A. Supplementary material

Supplementary data to this article can be found online at https://doi.org/10.1016/j.seppur.2024.129134.

References

[1] R.T. Mertens, S. Gukathasan, A.S. Arojojoye, C. Olelewe, S.G. Awuah, Next generation gold drugs and probes: chemistry and biomedical applications, Chem. Rev. 123 (2023) 6612–6667, https://doi.org/10.1021/acs.chemrev.2c00649.
[2] L. Zhang, J.-Q. Fan, Q.-Q. Zheng, S.-J. Xiao, C.-R. Zhang, S.-M. Yi, X. Liu, W. Jiang, Q.-G. Tan, R.-P. Liang, J.-D. Qiu, A 2D mesoporous hydrazone covalent organic framework for selective detection and ultrafast recovery of Au(III) from electronic waste, Chem. Eng. J. 454 (2023) 140212, https://doi.org/10.1016/j.cej.2022.140212.
[3] L. Ling, X. Huang, W. Zhang, Enrichment of precious metals from wastewater with core-shell nanoparticles of iron, Adv. Mater. 30 (2018), https://doi.org/10.1002/adma.201705703.
[4] Y. Ou, Y. Yang, L. Wang, K. Li, W. Gao, Y. Zhang, Q. Li, T. Jiang, A clean and efficient innovative technology for refractory sulfide gold ore: In situ gold extraction via self-generated thiosulfate, J. Clean. Prod. 419 (2023) 138280, https://doi.org/10.1016/j.jclepro.2023.138280.
[5] C. Owusu, S. Mensah, K. Ackah, R.K. Amankwah, Reducing preg-robbing in carbonaceous gold ores using passivative or blanking agents, Miner. Eng. 170 (2021) 106990, https://doi.org/10.1016/j.mineng.2021.106990.
[6] J.G. Dunn, A.C. Chamberlain, The recovery of gold from refractory arsenopyrite concentrates by pyrolysis-oxidation, Miner. Eng. 10 (1997) 919–928, https://doi.org/10.1016/S0892-6875(97)00074-5.
[7] A.D. Bas, F. Larachi, P. Laflamme, The effect of pyrite particle size on the electrochemical dissolution of gold during cyanidation, Hydrometallurgy 175 (2018) 367–375, https://doi.org/10.1016/j.hydromet.2017.12.016.
[8] K.L. Rees, J.S.J. Van Deventer, The role of metal-cyanide species in leaching gold from a copper concentrate, Miner. Eng. 12 (1999) 877–892, https://doi.org/10.1016/S0892-6875(99)00075-8.
[9] C.A. Johnson, The fate of cyanide in leach wastes at gold mines: An environmental perspective, App. Geochem. 57 (2015) 194–205, https://doi.org/10.1016/j.apgeochem.2014.05.023.
[10] G. Hilson, A.J. Monhemius, Alternatives to cyanide in the gold mining industry: what prospects for the future? J. Clean. Prod. 14 (2006) 1158–1167, https://doi.org/10.1016/j.jclepro.2004.09.005.
[11] Y. Lin, X. Hu, F. Zi, Thiocyanate facilitating thiosulfate extraction of gold via inhibiting formation of passive layer, Sustain. Mater. Techno. 40 (2024) e00878.
[12] J. McNeice, H. Mahandra, A. Ghahreman, Application of Biogenic Thiosulfate Produced by Methylophaga sulfidovorans for Sustainable Gold Extraction, ACS Sustain. Chem. Eng. 10 (2022) 10034–10046, https://doi.org/10.1021/acssuschemeng.2c02872.
[13] D.T. Sun, N. Gasilova, S. Yang, E. Oveisi, W.L. Queen, Rapid, selective extraction of trace amounts of gold from complex water mixtures with a metal-organic framework (MOF)/polymer composite, J. Am. Chem. Soc. 140 (2018) 16697–16703, https://doi.org/10.1021/jacs.8b09555.
[14] J. Ran, N. Wang, X. You, C. Wu, Q. Li, M. Gong, T. Xu, Guanidylated hollow fiber membranes based on brominated poly (2,6-dimethyl-1,4-phenylene oxide) (BPPO) for gold sorption from acid solutions, J. Hazard. Mater. 241–242 (2012) 63–72, https://doi.org/10.1016/j.jhazmat.2012.08.067.
[15] W. Zhan, Y. Yuan, B. Yang, F. Jia, S. Song, Construction of MoS_2 nano-heterojunction via ZnS doping for enhancing in-situ photocatalytic reduction of gold thiosulfate complex, Chem. Eng. J. 394 (2020) 124866, https://doi.org/10.1016/j.cej.2020.124866.

[16] W. Zhan, Y. Yuan, X. Yao, B. Yang, F. Jia, C. Lin, J.L. Arauz-Lara, S. Song, Efficient recovery of Gold(I) from thiosulfate solutions through photocatalytic reduction with Mn(II)-doped MoS_2, ACS Sustain. Chem. Eng. 9 (2021) 11681–11690, https://doi.org/10.1021/acssuschemeng.1c02160.
[17] K. Sasaki, I. Suyama, R. Takimoto, K.T. Konadu, H. Ichinose, J. Eksteen, Complete gold extraction and recovery from double refractory gold ores by thiourea after bio-oxidation, Hydrometallurgy 227 (2024) 106330, https://doi.org/10.1016/j.hydromet.2024.106330.
[18] B. Niu, E. Shanshan, Z. Xu, J. Guo, How to efficient and high-value recycling of electronic components mounted on waste printed circuit boards: Recent progress, challenge, and future perspectives, J. Clean. Prod. 415 (2023) 137815, https://doi.org/10.1016/j.jclepro.2023.137815.
[19] J. Ren, Z. Zhu, Y. Qiu, F. Yu, T. Zhou, J. Ma, J. Zhao, Highly selective recovery of gold from strong acidic wastewater with high-purity by self-driven capture, Chem. Eng. J. 479 (2024) 147585, https://doi.org/10.1016/j.cej.2023.147585.
[20] F. Li, J. Zhu, P. Sun, M. Zhang, Z. Li, D. Xu, X. Gong, X. Zou, A.K. Geim, Y. Su, H.-M. Cheng, Highly efficient and selective extraction of gold by reduced graphene oxide, Nat. Commun. 13 (2022) 4472, https://doi.org/10.1038/s41467-022-32204-4.
[21] Z. Dong, T. Jiang, B. Xu, J. Wu, Q. Li, Y. Yang, A comparative study of electrodeposition and sodium dithionite reduction for recovering gold in gold-rich solution from the adsorption of thiosulfate solution by ion exchange resin, Sep. Purif. Technol. 328 (2024) 125053, https://doi.org/10.1016/j.seppur.2023.125053.
[22] Q. Weng, S. Song, W. Zhan, X. Zhang, Z. Xiang, J. Gao, F. Jia, Novel recovery of a low-concentration gold thiosulfate complex through electroreduction via a walnut shell charcoal electrode, Green Smart Mining Eng. 1 (2024) 58–66, https://doi.org/10.1016/j.gsme.2024.03.004.
[23] W. Zhan, X. Zhang, Y. Yuan, Q. Weng, S. Song, M. de J. Martínez-López, J.L. Arauz-Lara, F. Jia, Regulating Chemisorption and Electrosorption Activity for Efficient Uptake of Rare Earth Elements in Low Concentration on Oxygen-Doped Molybdenum Disulfide, ACS Nano 18 (2024) 7298–7310, https://doi.org/10.1021/acsnano.4c00691.
[24] X. Liu, Y. Liu, Y. Wang, D. Yuan, C. Wang, J. Liu, Efficient electrosorption of uranium(VI) by B, N, and P co-doped porous carbon materials containing phosphate functional groups, J. Solid State Electr. 25 (2021) 2443–2454, https://doi.org/10.1007/s10008-021-05029-2.
[25] K. Kim, S. Cotty, J. Elbert, R. Chen, C. Hou, X. Su, Asymmetric redox-polymer interfaces for electrochemical reactive separations: synergistic capture and conversion of arsenic, Adv. Materi. 32 (2020), https://doi.org/10.1002/adma.201906877.
[26] M. Mao, T. Yan, G. Chen, J. Zhang, L. Shi, D. Zhang, Selective capacitive removal of Pb^{2+} from wastewater over redox-active electrodes, Environ. Sci. Technol. 55 (2021) 730–737, https://doi.org/10.1021/acs.est.0c06562.
[27] X. Zhang, W. Zhan, Q. Weng, S. Song, J. Luis Arauz-Lara, F. Jia, Electro-assisted sorption behavior and mechanism of low-concentration rare earth elements on carbon based materials, Appl. Surf. Sci. 664 (2024) 160224, https://doi.org/10.1016/j.apsusc.2024.160224.
[28] M. Mao, T. Yan, J. Shen, J. Zhang, D. Zhang, Capacitive removal of heavy metal ions from wastewater via an electro-adsorption and electro-reaction coupling process, Environ. Sci. Technol. 55 (2021) 3333–3340, https://doi.org/10.1021/acs.est.0c07849.
[29] Y. Du, M. Liu, Y. Liu, X. Li, Z. Huang, D. Ding, S. Yang, J. Feng, Y. Chen, R. Chen, Modulating the pore and electronic structure for targeted recovery of platinum: accelerated kinetic and reinforced coordination, J. Hazard. Mater. 469 (2024) 133913, https://doi.org/10.1016/j.jhazmat.2024.133913.
[30] H. Wang, X. Mi, Y. Li, S. Zhan, 3D graphene-based macrostructures for water treatment, Adv. Mater. 32 (2020), https://doi.org/10.1002/adma.201806843.
[31] R.G. Pearson, Hard and soft acids and bases, J. Am. Chem. so.c 85 (1963) 3533–3539, https://doi.org/10.1021/ja00905a001.
[32] C. Li, L. Tian, X. Yuan, H. Jiang, Z. Hu, Y. Yin, Review of acidic titanium-based oxygen evolution anode catalyst design: Mechanistic, compositional design, and research status, J. Alloys. Compd. 979 (2024) 173576, https://doi.org/10.1016/j.jallcom.2024.173576.
[33] M.M. Sabzehmeidani, S. Mahnaee, M. Ghaedi, H. Heidari, V.A.L. Roy, Carbon based materials: a review of adsorbents for inorganic and organic compounds, Mater. Adv. 2 (2021) 598–627, https://doi.org/10.1039/D0MA00087F.
[34] S. He, G. Chen, H. Xiao, G. Shi, C. Ruan, Y. Ma, H. Dai, B. Yuan, X. Chen, X. Yang, Facile preparation of N-doped activated carbon produced from rice husk for CO_2 capture, J. Colloid. Interf. Sci. 582 (2021) 90–101, https://doi.org/10.1016/j.jcis.2020.08.021.
[35] M. Mariana, A.K. H.P.S., E.M. Mistar, E.B. Yahya, T. Alfatah, M. Danish, M. Amayreh, Recent advances in activated carbon modification techniques for enhanced heavy metal adsorption, J. Water Process Eng. 43 (2021) 102221. DOI: 10.1016/j.jwpe.2021.102221.
[36] M.A. Chayid, M.J. Ahmed, Amoxicillin adsorption on microwave prepared activated carbon from Arundo donax Linn: Isotherms, kinetics, and thermodynamics studies, J. Environ. Chem. Eng. 3 (2015) 1592–1601, https://doi.org/10.1016/j.jece.2015.05.021.
[37] K. Chomiak, S. Gryglewicz, K. Kierzek, J. Machnikowski, Optimizing the properties of granular walnut-shell based KOH activated carbons for carbon dioxide adsorption, J. CO_2 Utili. 21 (2017) 436–443, https://doi.org/10.1016/j.jcou.2017.07.026.
[38] D. Lan, M. Chen, Y. Liu, Q. Liang, W. Tu, Y. Chen, J. Liang, F. Qiu, Preparation and characterization of high value-added activated carbon derived from biowaste walnut shell by KOH activation for supercapacitor electrode, J. Mater. Sci-Mater. El. 31 (2020) 18541–18553, https://doi.org/10.1007/s10854-020-04398-0.
[39] S. Zeng, F. Jia, B. Yang, S. Song, In-situ reduction of gold thiosulfate complex on molybdenum disulfide nanosheets for a highly-efficient recovery of gold from thiosulfate solutions, Hydrometallurgy 195 (2020) 105369, https://doi.org/10.1016/j.hydromet.2020.105369.
[40] K. Frikha, L. Limousy, J. Pons Claret, C. Vaulot, K.F. Pérez, B.C. Garcia, S. Bennici, Potential valorization of waste tires as activated carbon-based adsorbent for organic contaminants removal, Materials 15 (2022) 1099, https://doi.org/10.3390/ma15031099.
[41] M. Liu, C. Cai, J. Li, J. Zhao, W. Teng, R. Liu, Stöber synthesis of tannic acid–formaldehyde resin polymer spheres and their derived carbon nanospheres and nanocomposites for oxygen reduction reaction, J. Colloid. Interf. Sci. 528 (2018) 1–9, https://doi.org/10.1016/j.jcis.2018.05.070.
[42] T. Kesavan, M. Sasidharan, Palm spathe derived N-doped carbon nanosheets as a high performance electrode for Li-Ion batteries and supercapacitors, ACS Sustain. Chem. Eng. (2019), https://doi.org/10.1021/acssuschemeng.9b01261.
[43] A.A. Shiryaev, P. Pré, C. Pardanaud, V. Murzin, A. Averin, J.-N. Rouzaud, Microporosity and nanostructure of activated carbons: characterization by X-ray diffraction and scattering, Raman spectroscopy and transmission electron microscopy, Adsorption 29 (2023) 275–289, https://doi.org/10.1007/s10450-023-00406-x.
[44] M. Shi, D. Bao, S. Li, B. Wulan, J. Yan, Q. Jiang, Anchoring PdCu amorphous nanocluster on graphene for electrochemical reduction of N_2 to NH_3 under ambient conditions in aqueous solution, Adv. Energy. Mater. 8 (2018), https://doi.org/10.1002/aenm.201800124.
[45] B. Tang, L. Zheng, X. Dai, H. Chen, Nitrogen/oxygen co-doped porous carbons derived from a facilely-synthesized Schiff-base polymer for high-performance supercapacitor, J. Energy Storage 26 (2019) 100961, https://doi.org/10.1016/j.est.2019.100961.
[46] L. Wang, Y. Gao, Y. Chai, X. Sun, Recovery of rare earth by electro-sorption with sodium diphenylamine sulfonate modified activated carbon electrode, Sep. Purif. Technol. 292 (2022) 121005, https://doi.org/10.1016/j.seppur.2022.121005.
[47] T.S. Hui, M.A.A. Zaini, Potassium hydroxide activation of activated carbon: a commentary, Carbon Let. 16 (2015) 275–280, https://doi.org/10.5714/CL.2015.16.4.275.
[48] N. Boonraksa, E. Swatsitang, K. Wongsaprom, Electrochemical performance of KOH-activated lotus seedpods carbon, Mat. Sci. Eng. B 301 (2024) 117151, https://doi.org/10.1016/j.mseb.2023.117151.
[49] G. Fu, H. Li, Q. Bai, C. Li, Y. Shen, H. Uyama, Dual-doping activated carbon with hierarchical pore structure derived from polymeric porous monolith for high performance EDLC, Electrochim. Acta 375 (2021) 137927, https://doi.org/10.1016/j.electacta.2021.137927.
[50] C. Saka, BET, TG–DTG, FT-IR, SEM, iodine number analysis and preparation of activated carbon from acorn shell by chemical activation with $ZnCl_2$, J. Anal. Appl. Pyrolysis 95 (2012) 21–24, https://doi.org/10.1016/j.jaap.2011.12.020.
[51] M. Betancur, J.D. Martínez, R. Murillo, Production of activated carbon by waste tire thermochemical degradation with CO_2, J. Hazard. Mater. 168 (2009) 882–887, https://doi.org/10.1016/j.jhazmat.2009.02.167.
[52] P.V. Thitame, S.R. Shukla, Adsorptive removal of reactive dyes from aqueous solution using activated carbon synthesized from waste biomass materials, Int. J. Environ. Sci. Te. 13 (2016) 561–570, https://doi.org/10.1007/s13762-015-0901-3.
[53] M.M. Vukčević, A.M. Kalijadis, T.M. Vasiljević, B.M. Babić, Z.V. Laušević, M. D. Laušević, Production of activated carbon derived from waste hemp (Cannabis sativa) fibers and its performance in pesticide adsorption, Micropor. Mesopor. Mater. 214 (2015) 156–165, https://doi.org/10.1016/j.micromeso.2015.05.012.
[54] H. Yamada, H. Nakamura, F. Nakahara, I. Moriguchi, T. Kudo, Electrochemical study of high electrochemical double layer capacitance of ordered porous carbons with both meso/macropores and micropores, J. Phys. Chem. C 111 (2007) 227–233, https://doi.org/10.1021/jp063902g.
[55] J.L. Hammond, A.J. Gross, P. Estrela, J. Iniesta, S.J. Green, C.P. Winlove, P. G. Winyard, N. Benjamin, F. Marken, Cysteine-cystine redox cycling in a gold-gold dual-plate generator-collector microtrench sensor, Anal. Chem. 86 (2014) 6748–6752, https://doi.org/10.1021/ac501321e.
[56] P. Chen, P.R. Brito-Parada, S. Song, F. Jia, Efficient recovery of gold from low concentration $Au(S_2O_3)_2^{3-}$ solution by fabricating Ag/MoS_2 Ohmic contact, Appl. Surf. Sci. 639 (2023) 158155, https://doi.org/10.1016/j.apsusc.2023.158155.
[57] S. Zhou, X. Mo, W. Zhu, W. Xu, K. Tang, Y. Lei, Selective adsorption of Au(III) with ultra-fast kinetics by a new metal-organic polymer, J. Mol. Liq. 319 (2020) 114125, https://doi.org/10.1016/j.molliq.2020.114125.
[58] Y. Chen, F. Zi, X. Hu, Y. Lin, H. Du, J. Hu, P. Yang, Y. Zhang, B. Yang, The first effective utilization of activated carbon in gold thiosulfate system: a more eco-friendly, easier method for gold recovery and material regeneration, Miner. Eng. 155 (2020) 106441, https://doi.org/10.1016/j.mineng.2020.106441.
[59] Z. Feng, C. Zhu, Y. Meng, Z. Wang, Preparation of highly selective polyether sulfone /polym-phenylenediamine membrane for recovery of Au(III) from aqueous solutions, Chem. Eng. Res. Des. 189 (2023) 452–460, https://doi.org/10.1016/j.cherd.2022.11.029.
[60] C.-H. Yen, H.-L. Lien, J.-S. Chung, H.-D. Yeh, Adsorption of precious metals in water by dendrimer modified magnetic nanoparticles, J. Hazard. Mater. 322 (2017) 215–222, https://doi.org/10.1016/j.jhazmat.2016.02.029.
[61] H. Yu, F. Zi, X. Hu, Y. Nie, P. Xiang, J. Xu, H. Chi, Adsorption of the gold–thiosulfate complex ion onto cupric ferrocyanide ($CuFC^{)}$- impregnated activated carbon in aqueous solutions, Hydrometallurgy 154 (2015) 111–117, https://doi.org/10.1016/j.hydromet.2015.04.009.

[62] M. Fırlak, E.K. Yetimoğlu, M.V. Kahraman, Adsorption of Au(III) ions from aqueous solutions by thiol-ene photoclick hydrogels and its application to electronic waste and geothermal water, J. Water Process Eng. 3 (2014) 105–116, https://doi.org/10.1016/j.jwpe.2014.05.016.

[63] C. Liu, H. Zhang, Q. Wang, J. Wu, P. Chen, S. Song, C. Zhan, L. Wang, F. Jia, Efficient gold recovery from low concentrated $Au(S_2O_3)_2^{3-}$ solution through enhanced photocatalysis via photothermal and surface plasmon resonance assistance on MoS_2/MXene/Ag, Desalination 584 (2024) 117733, https://doi.org/10.1016/j.desal.2024.117733.

[64] Y. Liang, J. Li, P. Chen, C. Liu, J. Ge, S. Song, L. Cisternas, F. Jia, Enhanced gold recovery from the leaching solution by using porous activated carbon coated electrode: COMSOL simulation and experiments, Sep. Purif. Technol. 353 (2025) 128603, https://doi.org/10.1016/j.seppur.2024.128603.

[65] F. Yu, X. Bai, M. Liang, J. Ma, Recent progress on metal-organic framework-derived porous carbon and its composite for pollutant adsorption from liquid phase, Chem. Eng. J. 405 (2021) 126960, https://doi.org/10.1016/j.cej.2020.126960.

[66] M. Zhi, F. Yang, F. Meng, M. Li, A. Manivannan, N. Wu, Effects of pore structure on performance of an activated-carbon supercapacitor electrode recycled from scrap waste tires, ACS Sustain. Chem. Eng. 2 (2014) 1592–1598, https://doi.org/10.1021/sc500336h.